Mon. Not. R. astr. Soc. (1983) **203**, 1087–1098

Kinematic structure of planetary nebulae – II. The Eskimo, NGC 2392

N. K. Reay and P. D. Atherton *Astronomy Group, Blackett Laboratory, Imperial College, London SW7 2BZ*

K. Taylor *Anglo-Australian Observatory, PO Box 296, Epping, NSW 2121, Australia*

Received 1982 September 19; in original form 1982 July 12

Summary. Seeing limited two-dimensional kinematic data for the Hα λ 6536 Å and [N II] λ 6583 Å lines have been obtained across the planetary nebula NGC 2392 using a wide field imaging Fabry–Perot interferometer (TAURUS).

We have used the data to construct a three-dimensional model for the nebula which shows it to be two concentric spheroidal shells viewed along their major axes. The inner shell has an axial ratio of 2 and is expanding with a velocity of 65 km s^{-1}. Defined by the condensations, the outer shell has an axial ratio $\geqslant 1$ and a maximum expansion velocity ~ 75 km s^{-1}. The condensations are set in a region of tenuous [O III] emission which is expanding at ~ 30 km s^{-1}. Interior to the inner surface of the inner shell there appears to be a component which is at rest with respect to the central star. The form of Wilson's observed spectral line profiles can be explained qualitatively in terms of simple stratification effects.

1 Introduction

In the following we report on observations of the detailed kinematic structure of the envelope of NGC 2392. These are the result of an observational program the objectives of which are to study a number of well-resolved planetary nebulae which are known to have unusual kinematic features.

Kinematic studies of planetary nebulae have, in the past, been restricted to measurement of the gross expansion velocity (Wilson 1950; Bohuski & Smith 1974; Johnson 1977; Robinson, Reay & Atherton 1982) and to a handful of velocity field measurements with Fabry–Perot interferometers (Taylor 1977, 1979; Hicks, Phillips & Reay 1976; Atherton *et al.* 1979). From these latter studies in particular it has become clear how essential it is to obtain velocity field information down to seeing-limited resolution in order to specify models which account simply and successfully for the morphology of the nebular envelopes.

2 Previous observational work

NGC 2392 is a moderately bright high-excitation nebula with a well-developed double envelope structure (Curtis 1918; Aller 1964; Kaler 1974). The inner envelope is slightly elliptical in projection with a mean outer diameter of 13 arcsec. The faint outer envelope is also slightly elliptical. It has a mean overall diameter of 46 arcsec and has set in it a number of relatively bright condensations which give it a fragmentary appearance (Moore 1921). Spectroscopic observations show the inner envelope to be expanding at 54 km s^{-1} (Wilson 1948) and the mean radial velocity of the system to be +71 km s^{-1}.

From plates taken over a 50-yr period Liller, Welther & Liller (1966) and Liller (1965) found no evidence for angular expansion of either the inner or outer envelopes, although a subsequent series of measurements by Liller & Liller (1968) indicated a mean nebular expansion rate of 0.72 ± 0.06 arcsec $century^{-1}$. These figures compare with a predicted expansion rate of 4 arcsec $century^{-1}$ based on the measured expansion velocity of 54 km s^{-1} and a distance (Acker 1978) of 1 kpc. This discrepancy may be accounted for if:

(a) The envelope is a prolate ellipsoid of large axial ratio, with the major axis directed along the line-of-sight and expansion velocity proportional to distance from the star.

(b) The nebula is more distant than 1 kpc.

With expansion velocity proportional to distance from the star (Weedman 1968) and the major axis directed towards the observer, the expansion in the plane of the sky will be less than along the major axis. Adopting Weedman's (1968) axial ratio value of 3:1 for the inner envelope of NGC 2392, the measured 54 km s^{-1} expansion velocity if along the major axis implies an expansion velocity of 18 km s^{-1} in the plane of the sky, i.e. an angular expansion rate of ~1.2 arcsec $century^{-1}$ at a distance of 1 kpc. To obtain an angular expansion rate as low as 0.72 arcsec $century^{-1}$ (Liller & Liller 1968) requires either that the distance has been underestimated by a factor of 2 or the expansion velocity in the plane of the sky is 10 km s^{-1}, suggesting an axial ratio of 6:1, somewhat higher than values normally adopted. Also it is worth noting that although the central star of NGC 2392 is ejecting mass (Wilson 1948), the mass loss rate is almost certainly insufficient to compensate for the reduction in number density caused by the nebular expansion and incapable therefore of causing a reduction in the apparent expansion rate of the H II region. Taking available expansion velocity, distance and angular dimensions for NGC 2392 and assuming an electron density of $10^4 cm^{-3}$, the mass input to the nebula would have to be $\sim 7 \times 10^{-4} M_\odot$ yr^{-1} to maintain the density of the H II region. Pottasch (1982, private communication) has recently estimated the mass loss rate for the central star (based on *IUE* data) to be $\sim 10^{-5} M_\odot$ yr^{-1}. This mechanism, suggested by Zanstra (1953) and Schatzman & Kahn (1955) in relation to Galactic H II regions, will not therefore be significant in influencing the kinematics of NGC 2392.

3 Kinematic observations

We have used TAURUS, a new imaging Fabry–Perot system (Taylor 1978; Taylor & Atherton 1980; Atherton *et al.* 1982) to obtain emission line profiles for the lines [N II] λ 6583 Å and H I λ 6563 Å at 'seeing limited' spatial resolution over a 2 arcmin field centred on NGC 2392.

The observations were made using the SAAO 1.9-m telescope in 1980 February. The Image Photon Counting System (IPCS) area detector (Boksenberg 1972) was used with a pixel size (projected on to the sky) of 1.09 arcsec by 0.88 arcsec. At each of 70 wavelength intervals spaced by 0.065 Å (3 km s^{-1}) an image comprising 128 × 128 pixels was recorded at

a spectral resolution of 0.11 Å (i.e. ~5 km s^{-1}). The three-dimensional data array thus created (two spatial dimensions of approximately 2 arcmin by 1.8 arcmin and one spectral dimension of 4.5 Å) was then processed using the SERC STARLINK computer system to give both a series of monochromatic (5 km s^{-1}) velocity slices through the object and, by relating pixels from frame to frame, a velocity field across the nebular envelope. The calibration and data reduction procedures applied to TAURUS data are discussed in detail by Atherton *et al.* (1982) and by Pike *et al.* (1980).

4 Results and discussions

In Fig. 1 we show a sequence of velocity slices through NGC 2392 obtained by 'binning' individual [N II] λ6583 Å frames by 3 and selecting alternate binned frames in order to compress the data for display purposes. The sequence of frames covers a wavelength range of

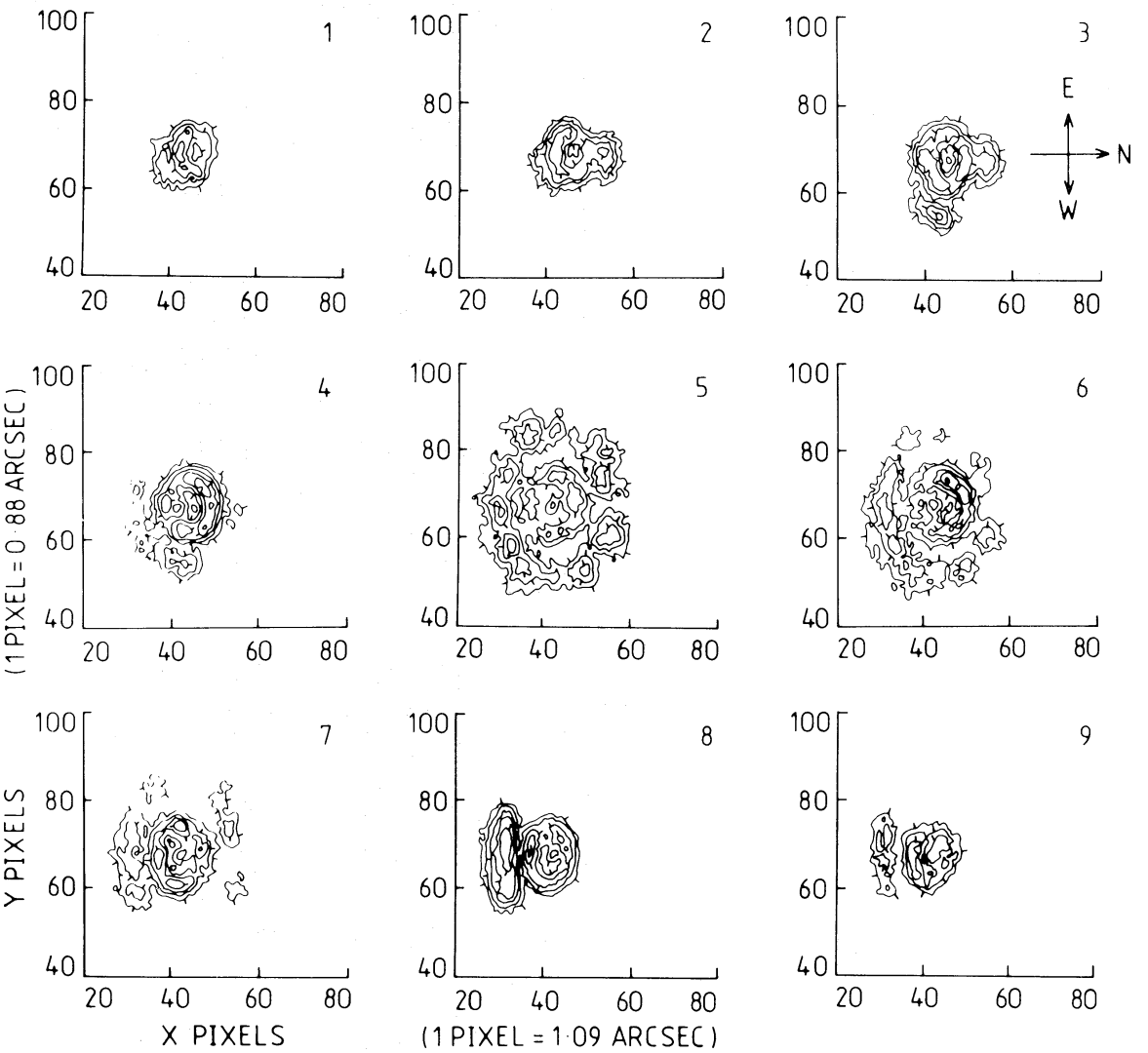

Figure 1. [N II] λ6583 Å. A sequence of monochromatic slices through NGC 2392 equivalent to viewing the nebula through 0.33 Å (15 km s^{-1}) passband filters spaced at wavelength intervals of 0.66 Å (30 km s^{-1}), wavelength decreasing with frame numbers. Note the prominent 'south bar' in frame 8, arising in material approaching along the line-of-sight and the relatively faint appearance of the inner envelope at the rest velocity of the object (frame 5). Markers on contours point in direction of decreasing intensity.

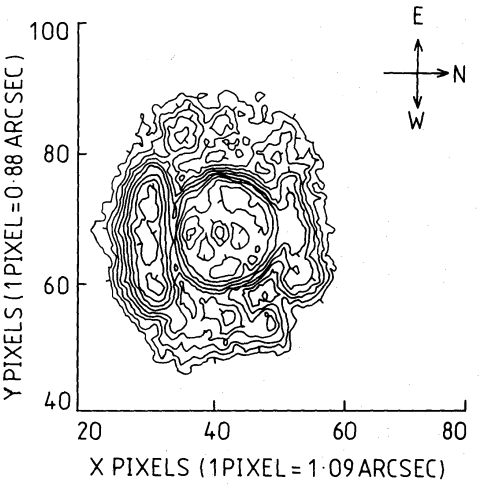

Figure 2. [N II] λ6583 Å. Addition of frames over an order of interference of the Fabry–Perot interferometer. The prominent 'south bar' and fainter 'north bar' are both clearly visible.

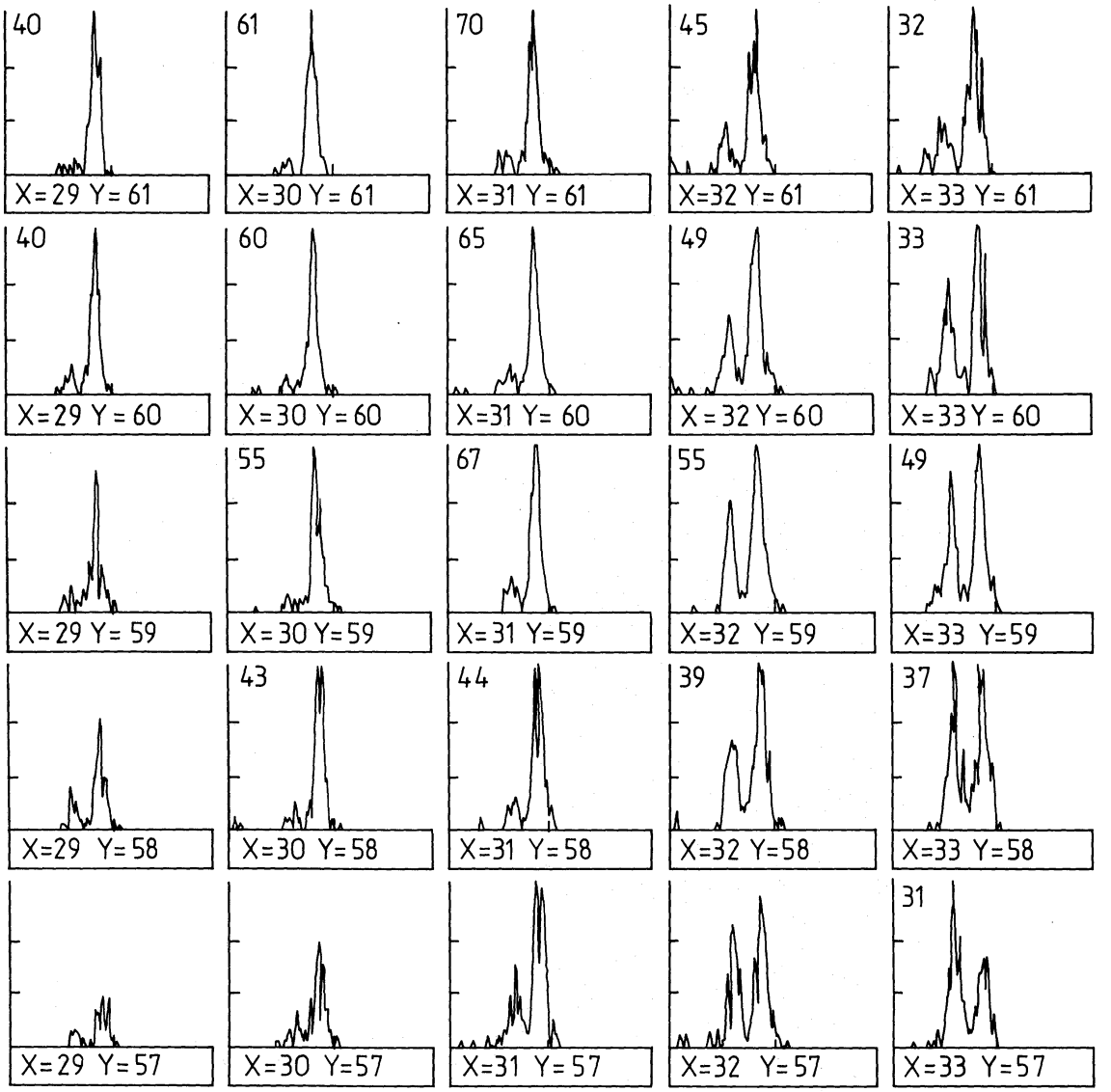

Figure 3. Sample spectra from the [N II] array. Wavelength range is 4.55 Å and scans from red to blue.

4.05 Å (185 km s^{-1}) equal to a complete 'free spectral range' for the 535 μm gap etalon used in the interferometer. It is equivalent to viewing the nebula through a series of 0.33 Å passband filters spaced at wavelength intervals of 0.66 Å.

Fig. 2 is a contour map obtained by adding together frames over one order of interference. It is in effect what would be observed through the order-sorting filter of width 12 Å located before the Fabry–Perot etalon.

In Fig. 3 we show a sample spectra for a small fraction of the data array. The spatial resolution is that of the pixel (1.09 × 0.88 arcsec) and the spectral resolution is 0.11 Å. Spectra of this quality are available across the entire envelope of NGC 2392; 16 384 in all although some register sky background only. Figs 4, 5 and 6 are samples of a comparable data set obtained for the H I λ 6563 Å emission line.

4.1 INNER ENVELOPE

The compact inner envelope appears in all frames, being of maximum projected diameter (13 arcsec) in the rest frame (frame 5 of Figs 1 and 4) and gradually diminishing in diameter

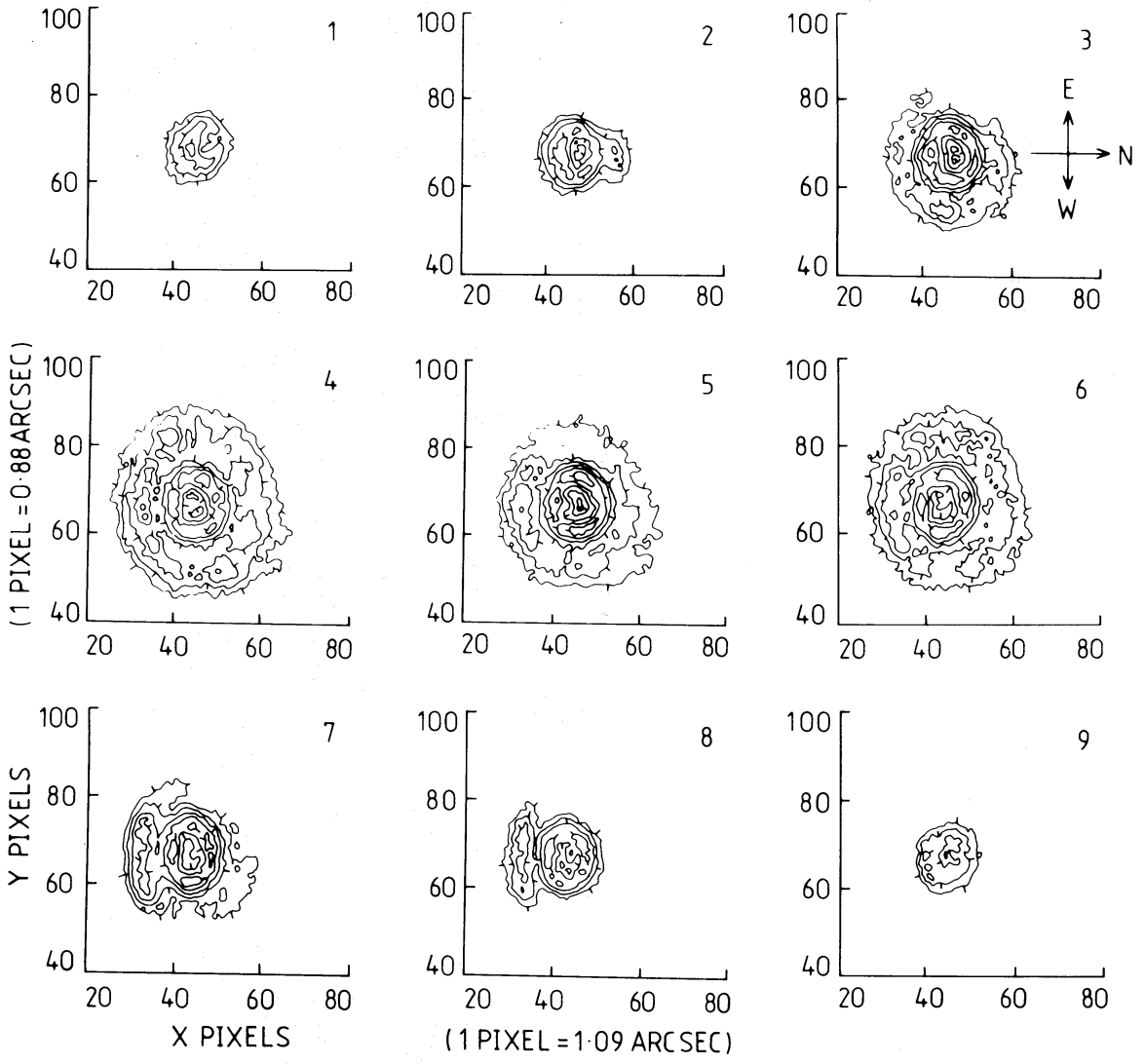

Figure 4. Hα λ 6583 Å. A sequence of monochromatic slices comparable with those for [N II] presented in Fig. 1. Note the relatively bright inner envelope at the rest velocity of the object (frame 5).

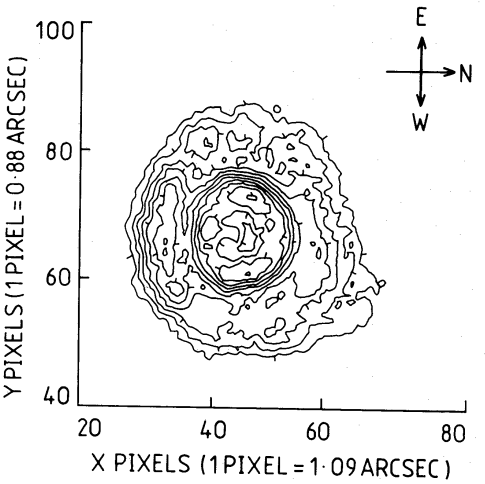

Figure 5. Hα λ 6563 Å. Addition of frames over an order of interference of the interferometer (4 Å). Distortion of the outer contour lines to the north-west of the object is due to multiple reflections in the interferometer.

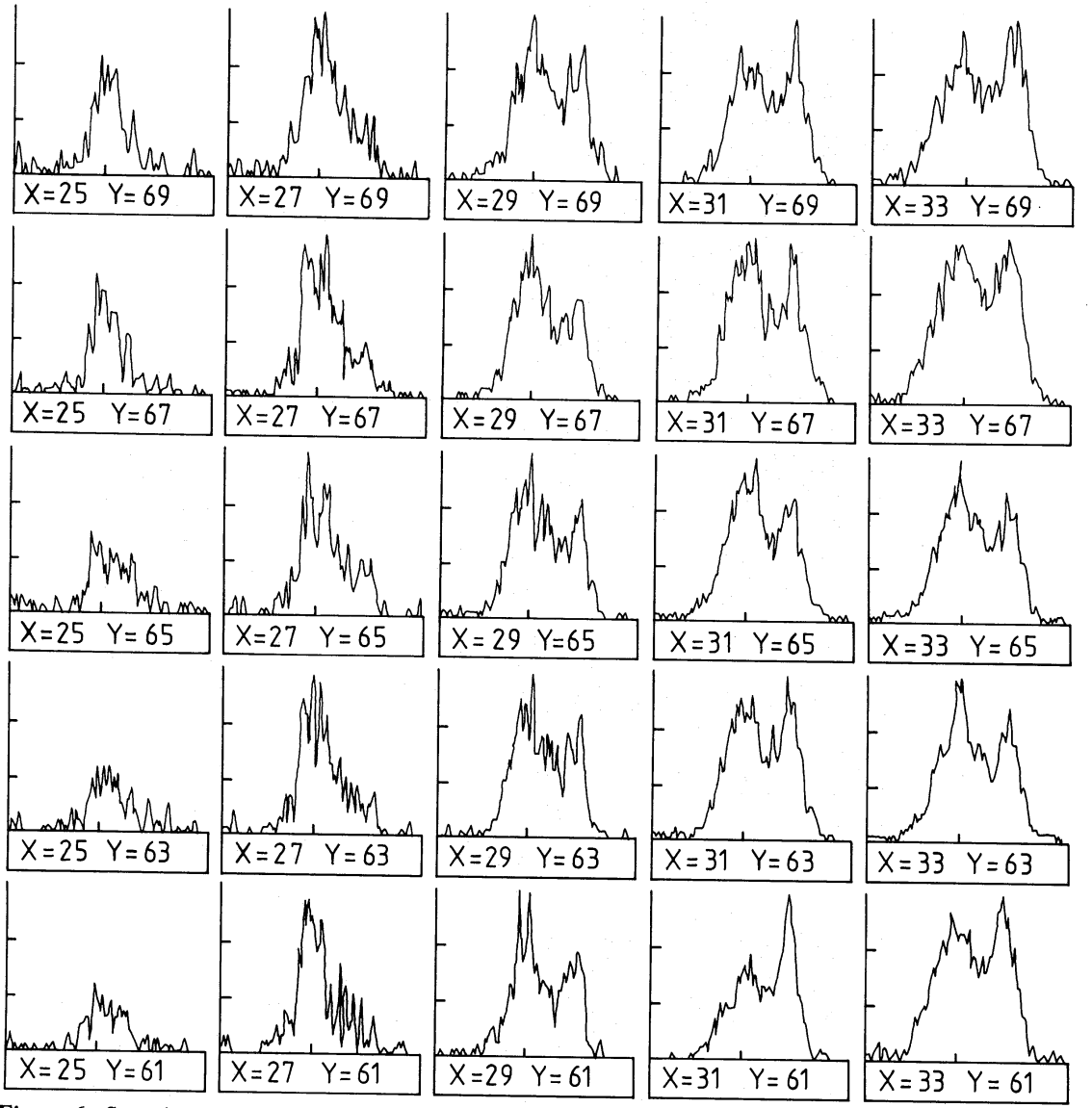

Figure 6. Sample spectra from the Hα array, binned by 2 to improve signal-to-noise ratio. Wavelength range is 4.55 Å and scans from red to blue.

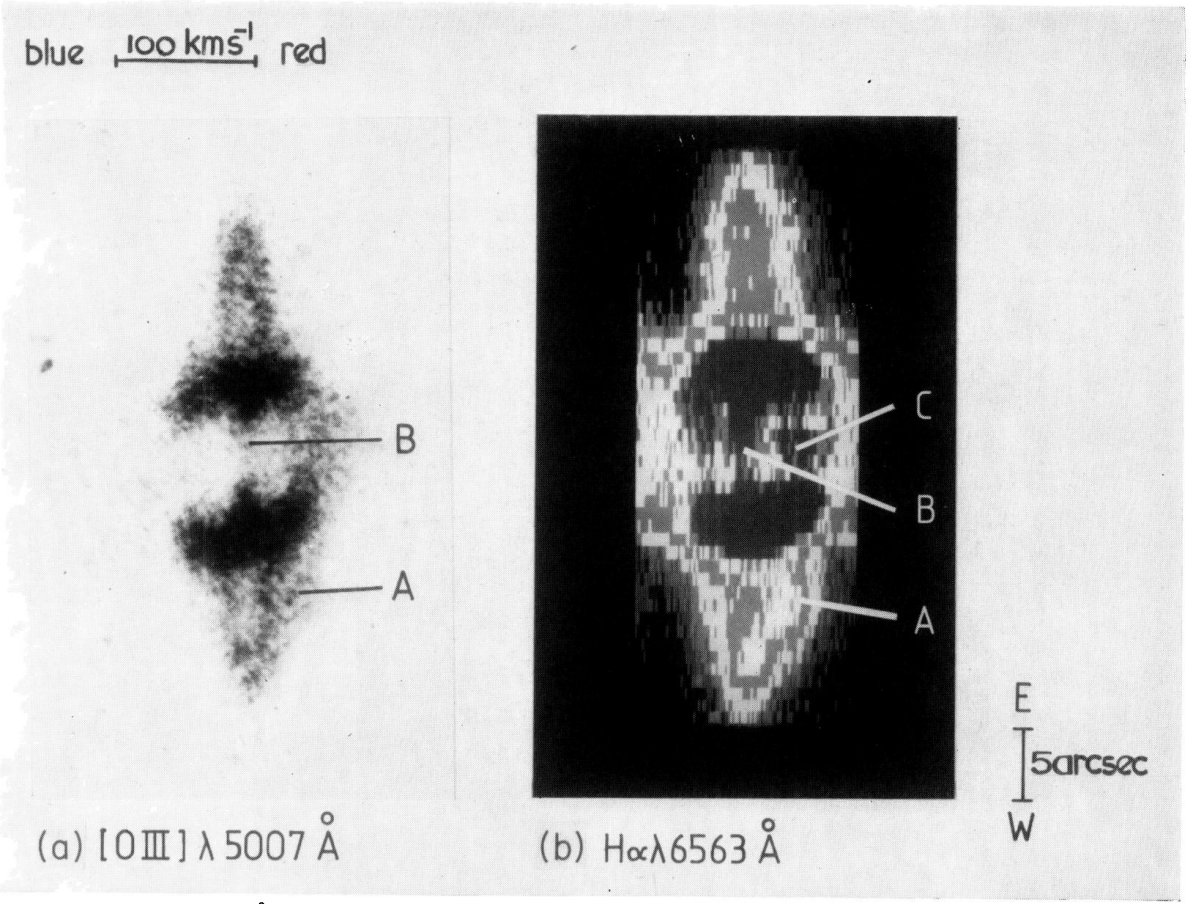

Plate 1. (a) [O III] λ5007 Å line profile recorded electronographically with spectrograph slit oriented E–W and passing through the centre of the object. Slit width was 0.5 arcsec. Maximum expansion velocity is ~65 km s^{-1}. (b) Hα λ6563 Å line profile generated from our new kinematic data. Both (a) and (b) show evidence for a relatively low expansion velocity (30 km s^{-1}) outer envelope in which are set condensations (*cf.* feature A) expanding at a higher velocity, and for a zero velocity HII, component inside the inner envelope (feature B). The Hα profile also shows evidence for a discrete condensation in the inner envelope (feature C).

[*facing page* 1092]

with wavelength away from the rest frame. Frames 3 and 7 are at approximately 60 km s^{-1} from the rest frame and the doughnut structure of the inner envelope is still clearly visible. This behaviour is taken as evidence that the inner envelope has a hollow shell structure and not a toroidal structure as proposed by Louise (1981), with a maximum expansion velocity somewhat greater than 60 km s^{-1}. The symmetry of the shell with respect to the rest-frame indicates that the line-of-sight is approximately along the major axis.

Frames 1 and 9 of Figs 1 and 4 therefore view the extreme far-side and near-side respectively of the inner envelope. They are spaced at 2.6 Å from the rest frame and indicate that material expanding at 120 km s^{-1} from the central star exists within the envelope. Inspection of pixels near the centre of the nebula confirms that the spectral lines are very broad, with well resolved 'wings' which extend out to ±120 km s^{-1} from the rest frame velocity. The broadening is consistent with there being a velocity gradient in the inner envelope caused, possibly, by initial ejection over a range of velocities.

In Plate 1 we show an [O III] λ 5007 Å line profile obtained with the 2.5-m Isaac Newton telescope at the Royal Greenwich Observatory compared with a synthetic Hα profile constructed from our new kinematic data. The slit orientation for the [O III] spectrum was east–west passing through the centre of the nebulae. Resolution along the slit was seeing limited to ~2 arcsec and spectral resolution is ~0.2 Å. The [O III] and Hα profiles are very similar, giving an inner evelope expansion velocity of 65 km s^{-1}. The expansion velocity falls to ~45 km s^{-1} at 5 arcsec from the centre and the effect of averaging over the central part of the nebula could therefore account for the expansion velocity value of 54 km s^{-1} previously measured. There is clear evidence in the profile for resolved condensations in both outer and inner envelope, and in both profiles for a zero velocity component inside the inner envelope.

A curious feature of the [N II] data (Fig. 1) is that the inner shell is very faint in the rest frame of the object and increases in brightness at longer and shorter wavelengths.

Anticipating the discussion in Section 5, this behaviour can be understood in terms of a prolate spheroidal inner shell, with the major axis along the line-of-sight, in which the level of ionization varies with distance from the star.

The rest frame therefore provides a view of the 'belt' of gas which is closest to the central star and hence most highly ionized. The 'caps' of [N II] emission which appear before and after the rest frame will arise in lower-excitation regions of the shell more distant from the central star. This behaviour is consistent with Wilson's (1948) observation that the high excitation [Ne V] λ 3346 Å and λ 3426 Å lines from the inner envelope are single and confined largely to the bright ring, whereas other lines have the fishtail structure characteristic of an expanding envelope.

4.2 OUTER ENVELOPE

At Hα the outer envelope appears to be the projection of a spheroidal hollow shell with a number of condensations including an exceptionally prominent 'bar' which is apparent in frames 7 and 8 of Fig. 4 and is clearly the result of material in the outer shell approaching along the line-of-sight. The [N II] data shows a similar but more exaggerated behaviour. The outer envelope is only prominent near the rest frame and the 'bar' (frame 8 of Fig. 1) is seen to be at a radius comparable with the radius at which other condensations appear in the rest frame. A similar but considerably weaker structure also exists to the north of the nebula (Figs 2 and 3).

Both the bright southern bar and the faint northern bar are relatively stronger in [N II] than Hα compared with the inner envelope. Another underexposed data array shows that the southern bar is also very bright at λ 6300 Å [O I], consistent with it having a relatively low electron temperature (Boeshaar 1974).

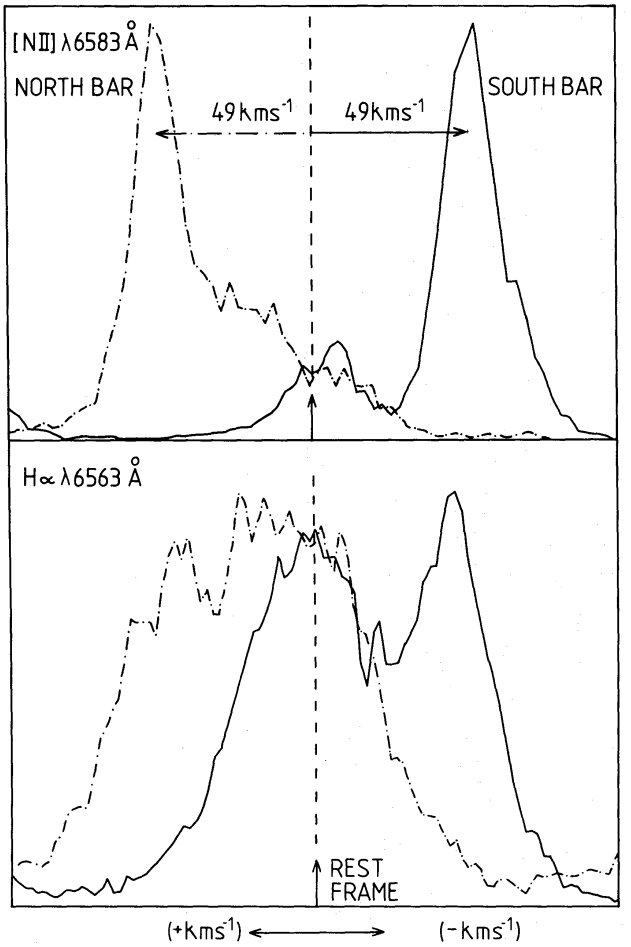

Figure 7. Sample spectra from the 'north bar' and 'south bar' superimposed to illustrate their symmetry. The rest frame component is clearly visible.

Fig. 7 shows typical spectra in Hα and [N II] at points in these 'bar' structures. Both Hα spectra have a strong component at the 'rest velocity' of the object, and the [N II] spectra show a distinct but relatively weaker component. From the [N II] data, the northern and southern 'bars' have velocities of +49 km s^{-1} and −49 km s^{-1} respectively with respect to the rest frame of the nebula. The Hα spectra give a broadly consistent picture although the strong rest frame component reduces the apparent velocity separation of the features.

In contrast to the relatively high velocity of the condensations, the background H II region sampled by the [O III] spectrum appears to be expanding at 30 km s^{-1} (Plate 1a). References to Fig. 1(a) of Louise (1981) shows both the inner and outer shells to be exceedingly uniform at the [O III] λ 5007 Å wavelength, in sharp contrast to their appearance in [N II] and Hα.

5 Geometric model for H II region

Using the original data from which Figs 1 and 4 were prepared we have obtained the mean diameters of the inner and outer envelopes as a function of a frame velocity with respect to the rest velocity frame. Diameters were measured between the peaks of the inner and outer envelopes at a number of position angles and the mean value was normalized to the mean rest-frame diameter for the inner envelope. The velocity was normalized to the expansion

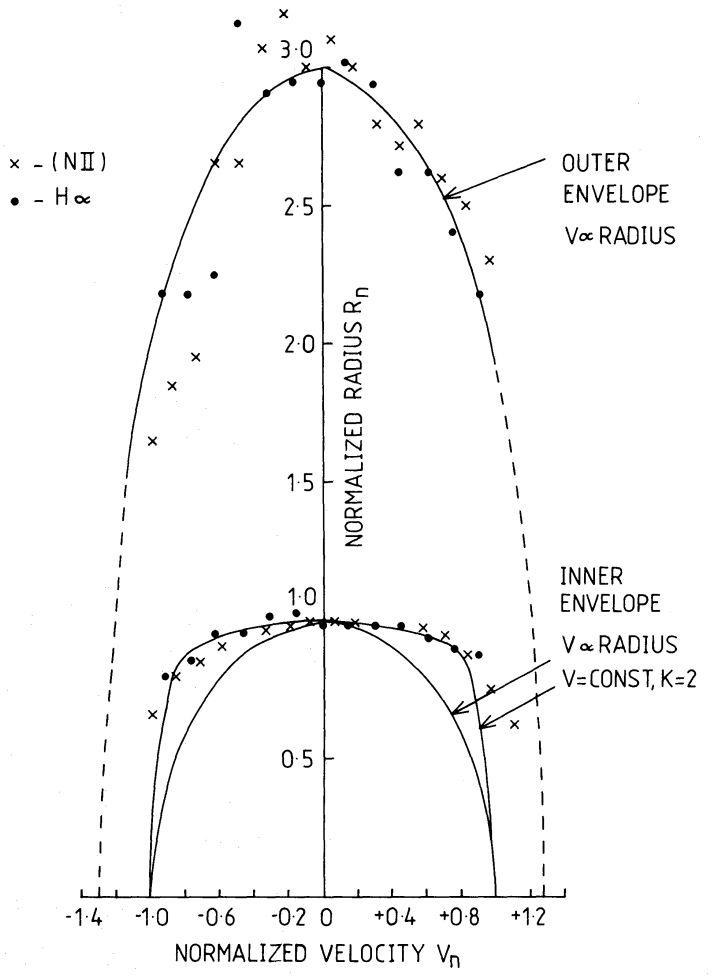

Figure 8. Envelope diameter versus frame velocity. V is envelope expansion velocity, K is axial ratio, (see text, Section 5).

velocity at the centre of the inner envelope (65 km s^{-1}). The results are shown in Fig. 8. This process is equivalent to obtaining a mean spectral line profile along a nebular radius on the assumption that the nebula is reasonably symmetric about the line-of-sight. Furthermore, the process weights heavily the condensations in the outer envelope as it is these features which are used to obtain a measure of the envelope diameter.

We have plotted for comparison in Fig. 8 theoretical curves for thin shell nebulae (major axis along line-of-sight), with a constant expansion velocity and with an expansion velocity which increases linearly with radius. The best fit to the inner envelope data points is given by a prolate spheroidal shell with an axial ratio of 2, expanding at a constant velocity. Any attempt to make velocity a strong function of radius depresses the theoretical curve below the data points.

The outer envelope data points are fitted either by a spherical (constant velocity) shell expanding at 75 ± 10 km s^{-1} ($V_n = 1.15 \pm 0.15$) or by a prolate shell with velocity proportional to distance from the star, the two cases being indistinguishable on the basis of our data.

That there appears to be a clear-cut separation of inner and outer shells (Figs 2 and 4) however, may be interpreted as evidence that the outer shell has an axial ratio > 1, with an major axis along the line-of-sight. The ring-like appearance of the outer shell would be enhanced as the axial ratio increased, especially if we assume that between the inner and outer boundaries of the outer shell the gas density is proportional to $r^{-\alpha}$ ($\alpha = 2$–3) (Phillips

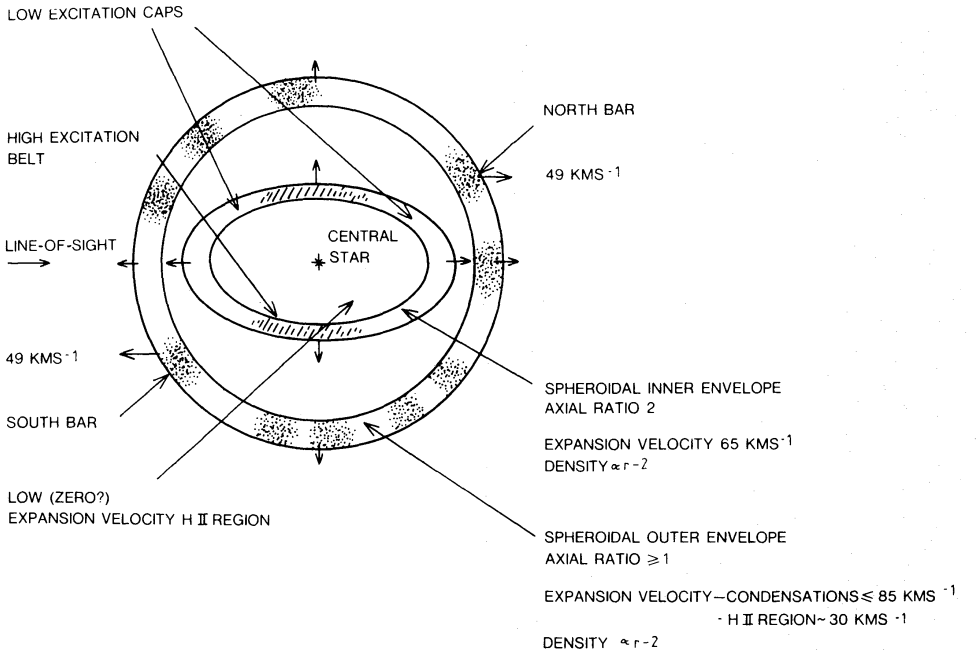

Figure 9. Model for NGC 2392 – schematic cross-section, (see text, Section 5).

& Reay 1977) where r is the distance from the central star. Arguments relating to the distance and size of NGC 2392 (see below) also suggest an outer envelope axial ratio significantly greater than 1.

Fig. 9 shows a schematic model for NGC 2392. The inner envelope is ellipsoidal with an axial ratio of 2 and the major axis directed along the line-of-sight. Expansion velocity at each point in the envelope is $\sim 65\ \mathrm{km\ s^{-1}}$ and the density between the inner and outer boundaries of the shell is constant. Also, there is evidence (Figs 1, 4 and Plate 1b) for resolved condensations within the inner envelope.

The 'belt' of gas in the inner shell (Fig. 9) near to the hot central star will be highly ionized and give the unshifted [Ne v] profiles observed by Wilson (1948) at the outer edge of the inner shell. Material towards the major axis will be in two lower ionization 'caps' and will give the split profiles typical of expanding spheroidal shells. The high excitation belt will also account for the low [N II] intensity in the inner shell in the rest frame of the object. (Fig. 1).

Internal to the inner boundary there appears to be a faint zero velocity H II component (Plate 1a and b).

The outer envelope defined by the condensations is also ellipsoidal with an axial ratio $\geqslant 1$, but otherwise undetermined. Comparison of Fig. 8 and Plate 1(a) shows that the [O III] data samples the uniform background H II region expanding at $\sim 30\ \mathrm{km\ s^{-1}}$, relative to which the condensations are moving. The zero velocity components in Fig. 7 would, in fact, arise as a consequence of viewing the edge of this slowly expanding H II region.

The bright 'north bar' and fainter 'south bar', along with a number of fainter condensations, are, we propose, the result of a symmetric ejection from the central star at an epoch early in the lifetime of the nebula. They are low temperature, high density regions (Boeshaar 1974) which are relatively bright in the low-excitation lines and very faint in He II, [Ne v] and [O III]. With an angular radius of approximately 22 arcsec and an expansion velocity of $30\ \mathrm{km\ s^{-1}}$ the [O III] region has a kinematic age of 3800 to 7600 yr assuming a distance of 1 kpc and an axial ratio of between 1 and 2. The condensation expansion velocity of

~ 75 km s^{-1} implies a kinematic age of 2500 yr, i.e. ejection at some considerable time after the outer shell.

The relatively weak shock associated with this process may be expected to result in enhancement of low-excitation nebular lines such as [N II] and [S II] (Brand & Mathis 1978).

6 Conclusion

NGC 2392 is an unusual double envelope nebula. Both envelopes are very uniform at [O III] λ 5007 Å but fragmented at Hα λ 6563 Å and [N II] λ 6583 Å.

The inner envelope is best fitted by a prolate spheroid of axial ratio 2 with the major axis orientation along or near to the lines-of-sight. Material on the minor axis near to the star is more highly excited than that along the major axis and the model accounts qualitatively for Wilson's (1948) observed line profile shapes. The shell has a uniform mean density and a constant expansion velocity ~ 65 km s^{-1}.

The outer envelope has a maximum [O III] expansion velocity of 30 km s^{-1} and a smooth density distribution inferred from the [O III] λ 5007 Å exposures of Louise (1981). Superimposed on the uniform outer shell there are a number of high density, low temperature condensations expanding at ~ 75 km s^{-1} from the central star. These condensations are contained within an ellipsoidal shell with axial ratios $\geqslant 1$ and, if ellipsoidal, with the major axis directed along or near to the line-of-sight.

Returning now to the problem of reconciling the model with measures of angular expansion by Liller & Liller (1968), it is clearly only possible to do so if the distance of the nebula is substantially greater than 1 kpc. An outer shell axial ratio of 2 would require a distance of >3 kpc and a spherical outer shell expanding at 75 km s^{-1} would need to be >6 kpc distant. Angular expansion velocity measurements are, of course, notoriously difficult to make and there remains the possibility that the expansion rate has been substantially underestimated.

Acknowledgments

We gratefully acknowledge the valuable contributions made to this program by Richard Hook and David Pike. We thank Howard Stephenson for his assistance at the telescope, and the Director and staff of the South African Astronomical Observatory for their hospitality. Data reduction was accomplished on the RGO node of the SERC STARLINK computer system.

References

Acker, A., 1978. *Astr. Astrophys. Suppl.*, **33**, 367.

Aller, L. H., 1964. *Numerical Data and Functional Relationship in Science and Technology*, Group VI, Bd I. Springer-Verlag, p. 566.

Atherton, P. D., Hicks, T. R., Reay, N. K., Robinson, G. J., Worswick, S. P. Phillips, J. P., 1979. *Astrophys. J.*, **232**, 786.

Atherton, P. D., Taylor, K., Pike, C. D., Harmer, C. F. W., Parker, N. Hook, R. N., 1982. *Mon. Not. R. astr. Soc.*, **201**, 661.

Boeshaar, G. O. 1974. *Astrophys. J.*, **187**, 283.

Bohuski, T. J. & Smith, M. G., 1974. *Astrophys. J.*, **193**, 197.

Boksenberg, A., 1972. *Auxiliary Instrumentation for Large Telescopes, Proc. ESO/CERN Conference, Geneva.* p. 205.

Brand, P. W. J. L. & Mathis, J. S., 1978. *Astrophys. J.*, **223**, 161.

Curtis, H. D., 1918. *Publs Lick Obs.,* **13,** P1 XI.
Hicks, T. R., Phillips, J. P. & Reay, N. K., 1976. *Mon. Not. R. astr. Soc.,* **176,** 409.
Johnson, H. M., 1977. *Astrophys. J.,* **208,** 127.
Kaler, J. B., 1974. *Astr. J.,* **79,** 594.
Liller, M. A. & Liller, W., 1968. *IAU Symp. No. 34,* eds Osterbrock, D. E. & O'Dell, C. R. Reidel, Dordrecht, Holland.
Liller, M. A., Welther, B. L. & Liller, W., 1966. *Astrophys. J.,* **144,** 280.
Liller, W., 1965. *Publs astr. Soc. Pacific,* **77,** 25.
Louise, R., 1981. *Astrophys. Space Sci.,* **79,** 229.
Moore, J. H., 1921. *Publs astr. Soc. Pacific,* **33,** 3.
Phillips, J. P. & Reay, N. K., 1977. *Astr. Astrophys.,* **59,** 91.
Pike, C. D., Taylor, K., Atherton, P. D. & Hook, R. N., 1980. *JPL Conference on Image Processing.*
Robinson, G. J., Reay, N. K. & Atherton, P. D., 1982. *Mon. Not. R. astr. Soc.,* **199,** 649.
Schatzman, E. & Kahn, F. D., 1955. *Gas Dynamics of Cosmic Clouds,* p. 163. North Holland, Amsterdam.
Taylor, K., 1977. *Mon. Not. R. astr. Soc.,* **181,** 475.
Taylor, K., 1978. *Proc. 4th Int. Coll. on Astrophysics, Trieste,* p. 469, ed. Hack, M.
Taylor, K., 1979. *Mon. Not. R. astr. Soc.,* **189,** 511.
Taylor, K. & Atherton, P. D., 1980. *Mon. Not. R. astr. Soc.,* **191,** 675.
Weedman, D. W., 1968. *Astrophys. J.,* **153,** 49.
Wilson, O. C., 1948. *Astrophys. J.,* **108,** 201.
Wilson, O. C., 1950. *Astrophys. J.,* **111,** 279.
Zanstra, H., 1953. *Observatory,* **73,** 198.